International Journal of Social Science Research and Review

http://ijssrr.com
editor@ijssrr.com
Volume 6, Issue 1
January, 2023
Pages: 320-327

Microwave Absorbing Improvement of Barium M-Hexaferrite by Ni Doping

Ary Lestari; Kasim; Mala Utami; George Royke Deksino

Faculty of Defense Technology, Republic of Indonesia Defense University, Indonesia

E-mail: ary.lestari@tp.idu.ac.id; kasim@tp.idu.ac.id; mala.utami@tp.idu.ac.id; georgeroydeksino@gmail.com

http://dx.doi.org/10.47814/ijssrr.v6i1.765

Abstract

Variations of the doping ion Ni x = 0, 0.2, 0.4, and 0.6 have been successfully synthesized on Barium M-Hexaferrit (BaM) magnetic material using the solid-state reaction method and sintered at 1000 oC for 6 hours. X-Ray Diffraction (XRD), Scanning Electron Microscopy (SEM), and Vector Network Analyzer (VNA) were used to analyze phase changes and crystal size, morphological structure, and microwave absorption coefficients, respectively. The largest BaM phase was achieved at BaM x = 0.6, 92.23%, with a crystal size of 54,273 nm. Although BaM's surface morphological structure exhibits a uniform distribution of particles, some agglomerated particles form due to magnetic dipole interactions among particles. The addition of an Ni doping ion variation improves the reflection loss and absorption bandwidth in the X-Band of 8.2-12.4 GHz. The highest reflection loss of -29.7 dB and the highest absorption of 75.82% were recorded in the BaM x 0.6 phase over the frequency range of 9.66-10.93 GHz. According to the research findings, applying variations of the Ni doping ion to BaM material tends to increase the material's microwave absorption potential.

Keywords: *Barium Hexaferrite; Microwave Absorption; Reflection Loss*

Introduction

The third industrial revolution, which began in 1976, led to the development of the internet and wireless digital technologies. This has catalyzed the advancement of telecommunications technology. The growing number of communication service providers increases the density of electromagnetic waves radiated in the earth's atmosphere. This has a negative effect on electronic component performance (Suntoro, 2021) and human health (Wirapraja, 2018). To overcome this issues, a technology for electromagnetic wave radiation absorption into the environment has been developed (Malhotra, 2015). This technology results in developing a substance known as intelligent magnetic material. This intelligent magnetic material is a wave-absorbing material that can be used to protect against electromagnetic interference (EMI) and as Radar Absorbing Materials (RAM) (Rafeekali, 2015). By converting electromagnetic waves into heat energy with magnetic and dielectric properties, absorber material is used to lower the wave energy emitted by the EMI source. In general, a suitable absorbing material for electromagnetic waves must have high permeability and permittivity (Sulistyo, 2012) and a low reflectance loss value (Tripathi, 2015)

The chemical symbol for barium M-Hexferrite is BaM, and it has a stoichiometric hexagonal structure (Simbolon, 2019). Barium M-hexaferrite is a permanent magnet that exhibits strong magnetic anisotropy, chemical stability, saturation magnetization, and a high coercivity field (H. Syahrul, 2015). The high coercivity field value in BaM material results in a rise in its anisotropic properties, which reduces its absorption ability. To alter the anisotropic characteristics of BaM, doping with different divalent ions is required (Sahlam, 2018). Co, Zn, Ti, and Ni are frequently employed as BaM doping ions (Sholihah, 2012). Nickel (Ni) is a silver-white ferromagnetic metal. Nickel is a transition metal with an ionic radius and electron configuration identical to Fe^{3+} ions in the BaM structure (Priyono, 2013).

Numerous investigations have concentrated on adjusting hexaferrite by cation modification of the magnetic properties of Fe^{3+} ions (R. C. Pullar, 2012). Numerous methods, including coprecipitation (K.S. Moghaddam), sol-gel (M. Han, 2009), mechanical combustion (Ataie, 2007), molten ammonium nitrate (U. Topal, 2007), citrate-nitrate gel burning (S. Chaudhury, 2008), and solid reaction (Manawan, 2014), have been utilized for this purpose. Due to its ease of operation and little experimental equipment, the latter method has been applied in this study. The majority of ion doping on BaM has been done to reduce its magnetic saturation and coercivity, including Mn^{3+} (K. Lee, 2009), La^{3+} (Seifert, 2009), Cu^{2+}/Zn^{2+} [A. M. Cholifah, 2018 & Ramadhan, 2018), and numerous other combinations. Doping resulted in a significant increase in absorption. Thus, this research examined the effect of doping Ni x = 0, 0.2, 0.4, and 0.6 on the magnetic properties of BaM as a microwave absorber.

Materials and Methods

Preparation. All of the materials are commercial and with no further purification, including Barium Chloride Dyhidrat ($BaCl_2.2H_2O$, Merck ≥ 99%), Ferrite (Fe_2O_3, Merck ≥ 99%), and Nickel Sulfate ($NiSO_4$, Merck ≥ 99%). Later, four BaM samples with doping ion Ni x = 0, 0.2, 0.4, and 0.6 will be prepared with 10 grams each. The following stoichiometry was used to determine the composition of the materials.

$$BaCl_2.2H_2O + Fe_2O_3 + NiSO_4 \rightarrow BaFe_{(12-x)}Ni_xO_{19} + \gamma$$

The mass of each material was calculated using the molecular weight of each material and mathematical comparisons. The findings of the calculation of the composition of the BaM material are provided in Table 1.

$$Mr = \sum Ar$$

$$gram\ y = \frac{gram\,(BaFe_{12-x}Ni_xO_{19})}{Mr\,(BaFe_{12-x}Ni_xO_{19})} \times Mr\ y$$

Where Mr is relative molecular mass, Ar is relative atomic mass, x is the variation of Ni doping (x= 0, 0.2, 0.4, and 0.6), and y is BaM material ($BaCl_2.2H_2O$, Fe_2O_3, and $NiSO_4$).

Table 1. Mass composition of basic material BaM

Sample Code	Materials Mass (gram)			Molecule of BaM
	$BaCl_2.2H_2O$	Fe_2O_3	$NiSO_4$	
BaM x 0	2.198	8.620	0	$BaFe_{12}O_{19}$
BaM x 0.2	2.197	8.473	0.278	$BaFe_{11,8}Ni_{0,2}O_{19}$
BaM x 0.4	2.196	8.325	0.556	$BaFe_{11,6}Ni_{0,4}O_{19}$
BaM x 0.6	2.195	8.177	0.834	$BaFe_{11,4}Ni_{0,6}O_{19}$

Synthesis of BaM. Barium M-Hexaferrite was synthesized by the solid reaction method of H. Li et al. (2021). The basic material is ground separately and sieved using a 260-mesh sieve (260 holes in 1 inch). The basic material was weighed according to the mass composition determined and then ground in a planetary ball mill for 6 hours with deionized water. The ratio of balls to powder was 10:1. After that,

the mixture was dried in an oven at 110 °C and compacted in the shape of pellets with a thickness of 1.5 mm with 3% Polyvinyl Alcohol (PVA) as a binder sintered at 1000 °C for 6 hours. The sintering temperature of 1000 °C was chosen because this temperature allowed the formation of the BaM primary phase (Pullar, 2012). The pellets were then cooled in a desiccator and ground to be ready for characterization.

Characterization. To determine the quality and quantity of the obtained sample phase, X-Ray Diffraction (XRD) with Cu-K_α radiation (λ = 0.15418 nm) was used at an angle of 2θ between 20°-70°. Scanning Electron Microscopy (SEM, Tescan 2000 watt) was used to characterize the morphology. A Vector Network Analyzer (VNA, Advantest R3770-20 GHz) was used to analyze material absorption and absorption frequency bandwidth.

Results and Discussion

Figure 1. BaM pellet x = 0.6 (a) before sintering and (b) after sintering (T = 1000 °C)

As seen in Figure 1, the sintering process changes the color of the pellets from dark red to blackish brown. The color change is induced by temperature changes (*thermochromic properties*) caused by the loss of many oxygen atoms from the crystal lattice, resulting in an excess of negative charge in the crystal lattice and hence a different color (Bahtiar, 2010) and the formation of bonds between particles and the release of some contaminants (A. Doyan et al., 2015).

XRD Characterization. The BaM sample's crystalline phase was determined using X-Ray Diffraction with Cu K_α (λ = 0.15418 nm). $BaFe_{12}O_{19}$ and Fe_2O_3 are the phases formed. The hexagonal structure of the $BaFe_{12}O_{19}$ phase is characterized by the presence of a P group of 63/mmc. The COD (Crystallography Open Database) database, PDF 00-100-8326, was used to identify all of the substituted BaM peaks (x = 0.2, 0.4, and 0.6) that were in almost the same position as the unsubstituted BaM (x = 0). The BaM precursor will increase activation energy during the sintering process, allowing it to vibrate and arrange the structure in a more stable state. The atoms can diffuse interstitial or by substitution with one another until a stable and ordered phase is formed. $BaFe_{12}O_{19}$ dominated at positions 2θ = 33.99°, 37.85°, 39.56°, 56.63°, 64.46°, and 68.82°, while Fe_2O_3 was the highest secondary phase at position 2θ = 33.13°.

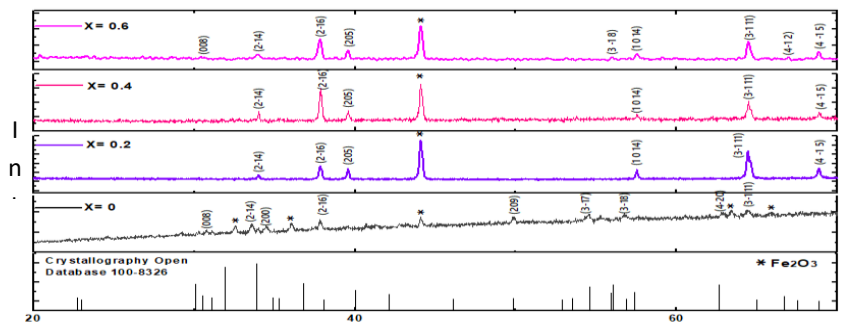

2 Theta

Figure 2. XRD pattern for $BaFe_{12-x}Ni_xO_{19}$

At BaM x = 0 (in the lack of the Ni doping ion), 29.35% Fe_2O_3 secondary phase remains. At BaM x = 0.2, 0.4, and 0.6 (substituted Ni doping ion), a secondary Fe2O3 phase also remains. This suggests that the heating process at 1000 ^oC with sintering for 6 hours could not completely incorporate the mass flow of Fe_2O_3 compounds. At x = 0.2, 0.4, and 0.6, the phase of the Fe_2O_3 peak dropped from four to one (Figure 2), however at BaM x = 0.6, the $BaFe_{12}O_{19}$ composition increased significantly to 92.23%.

Table 2. Composition of BaM and Fe_2O_3

Sample	Peak Intensity of $BaFe_{12}O_{19}$ (a.u.)	Peak Intensity of Fe_2O_3 (a.u.)	Total Peak Intensity (a.u.)	Composition of $BaFe_{12}O_{19}$ (%)	Composition of Fe_2O_3 (%)
$BaFe_{12}O_{19}$	16853	7000	23853	70.65	29.35
$BaFe_{11.8}Ni_{0.2}O_{19}$	13328	6687	20015	66.60	33.40
$BaFe_{11.6}Ni_{0.4}O_{19}$	7902	3704	11606	68.10	31.90
$BaFe_{11.4}Ni_{0.6}O_{19}$	890	75	965	92.23	7.77

Further quantitative analysis was performed to investigate the effect of Ni doping ion variation on the crystal size of BaM. The Scherrer formula was used to determine the crystal size.

$$D = \frac{k\lambda}{B\ Cos\ \theta_B}$$

Where D is the crystal size (nm), λ is the x-ray wavelength used (rad), θ_B denotes the Bragg angle, B denotes the FWHM (Full Width at Half Maximum) of a selected peak at 2θ x (π/180), and k denotes a material constant (k = 0.9).

Table 3. Crystal size of $BaFe_{12-x}Ni_xO_{19}$

Sample		Crystal Size (nm)
Molecule	Code	
$BaFe_{12}O_{19}$	BaM x 0	17.835
$BaFe_{11.8}Ni_{0.2}O_{19}$	BaM x 0.2	48.647
$BaFe_{11.6}Ni_{0.4}O_{19}$	BaM x 0.4	51.228
$BaFe_{11.4}Ni_{0.6}O_{19}$	BaM x 0.6	54.273

The BaM x = 0 phase has a crystal size of 17,835 nm, while the BaM x = 0.2, 0.4, and 0.6 phases with Ni-doped ions have crystal sizes of 48,647, 51,228, and 54,273 nm, respectively. After Ni doping with an ion, the crystal size of BaM increased. Additionally, variations in Ni doping ions increase in crystal size. Doping ions enable the substitution of Ni^{2+} ions for Fe^{3+} ions. The radius of the Ni^{2+} ion is larger than the radius of the Fe^{3+} ion, which results in a larger diffraction distance between the lattices when the Ni^{2+} ion substitutes for the Fe^{3+} ion.

Morphology Characterization. The results of SEM characterization revealed the morphological structure of BaFe12-xO_{19}. The surface morphology of the $BaFe_{12-x}Ni_xO_{19}$ sample is shown in Figure 3. The increase in grain size before and after the addition of the Ni doping ion resulted in the formation of a BaM magnetic phase with a low degree of homogeneity. At x = 0, BaM compounds are represented by small hexagonal grains, some of which are shaped like rice grains (rice-shaped), whereas large and thin hexagonal pieces represent Fe_2O_3 compounds. This assumption was supported by qualitative and quantitative XRD analysis, which revealed the formation of dominant BaM peaks and secondary Fe_2O_3 peaks. However, the intensity of Fe_2O_3 was greater than the intensity of BaM, with the presence of a single phase of Fe_2O_3 with high intensity.

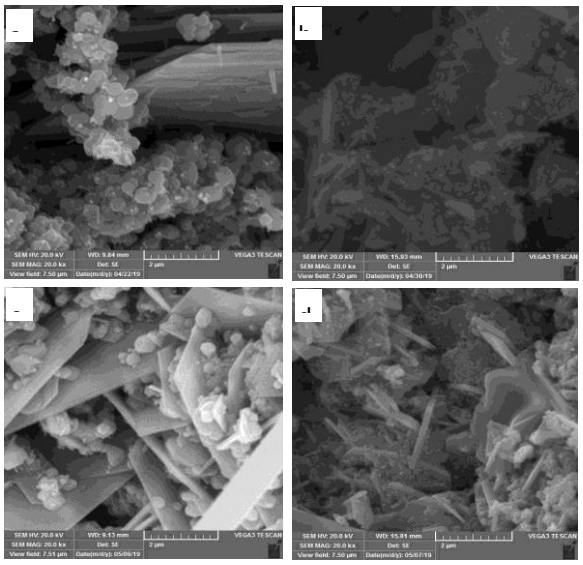

Gambar 3. SEM morphology of $BaFe_{(12-x)}Ni_xO_{19}$ with 20.000 magnification, (a) $BaFe_{12}O_{19}$, (b) $BaFe_{11.8}Ni_{0.2}O_{19}$, (c) $BaFe_{11.6}Ni_{0.4}O_{19}$, (d) $BaFe_{11.4}Ni_{0.6}O_{19}$

The crystal morphology of BaM is still not evident, as is the material's size, with certain sections adhering to one another and grains and pores clumping together (Joon, 2008). Agglomerated particles are possible as a result of particles. The grain size of the final material will affect its magnetic properties. According to Zebua (2002), grain size and grain size distribution have a significant effect on magnetic properties such as remanent induction (B) and coercive field (H_C). According to a magnetic susceptibility test conducted by Ma'rifat (2019) with Ni substituted BaM at x = 0.4, the greatest susceptibility value was 16277.164 x 10^{-8} m^3/Kg, classifying it as ferromagnetic.

VNA Characterization. The absorption properties of Barium M-Hexaferrite with various Ni-doping ions were determined using a Vector Network Analyzer (VNA). The measurements were carried out in the x-band frequency range, namely 8-12 GHz. In general, microwave bands share specific characteristics and are used for various purposes. Characterization with VNA yielded data in the form of scattering parameters, which are then used to generate an output in a frequency-dependent Reflection Loss (RL) curve.

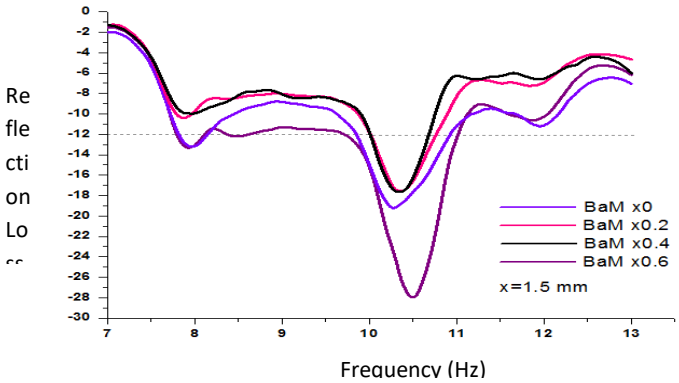

Figure 4. Reflection loss curve of $BaFe_{12-x}Ni_xO_{19}$

The results of the VNA test are shown in Figure 4, which is a graph of the reflection loss of BaM as a function of frequency. The color difference on each curve line indicates the variations x = 0, 0.2, 0.4, and 0.6. Absorption valleys are generated due to absorption; the deeper and wider the absorption valleys formed, the greater the absorption ability of the RAM material used (Awalin, 2017).

The reflection loss of the BaM x 0 material is -19.6 dB with an absorption power of 66.28%, which means that 33.72% of the total wave applied to the material will be reflected and/or transmitted. The BaM x = 0.2 and 0.4 samples exhibit identical reflection losses of -18.5 dB with 60.34 and 63.88% absorption powers, respectively. This is most likely since the dominant phase of Barium Hexaferrite is not well-formed. This is supported by the decreased crystalline intensity and composition of BaM in the XRD test results, which affects the microwave absorption properties. The BaM x 0.6 sample has the greatest variance, as demonstrated by the deepest absorption valley at -29.7 dB reflection loss and 75.82% absorption capacity at 10.5 GHz.

Table 4. Reflection loss value of $BaFe_{12-x}Ni_xO_{19}$

Sample	Reflection Loss (dB)	Absorption Coefficient (%)	Absorption band (GHz)
BaM x 0	-19.6	66.28	9.84 - 10.88
BaM x 0.2	-18.5	60.34	10.03 - 10.77
BaM x 0.4	-18.5	63.88	10.03 - 10.70
BaM x 0.6	-29.7	75.82	9.66 - 10.93

A material with good absorption will also have a broad absorption band, as it will be able to absorb microwaves over a wide frequency range. Because it is the highest absorption bandwidth range, the absorber bandwidth is measured at a reflection loss of -12 dB. Additionally, the most considerable absorbent bandwidth is found in the BaM x = 0.6 material with a frequency range of 9.66 GHz to 10.93 GHz (1.27 GHz). BaM x 0.6 material will be used as a microwave absorbent material more than unsubstituted or substituted BaM material with a lesser variation of Ni doping ion.

Conclusions

The solid-state reaction method was successfully applied to synthesize a $BaFe_{12-x}Ni_xO_{19}$ / BaM material with varied Ni doping ions (x = 0, 0.2, 0.4, and 0.6). At x = 0.6, a $BaFe_{12}O_{19}$ phase was formed with a composition of 92.23%. The addition of doping ion variations also affects the increased crystal size of BaM caused by the substitution of Ni^{2+} ions in the Fe^{3+} ion positions. This treatment enhances the material's ability to absorb microwaves in the X-Band region. The highest reflection losses of -29.7 dB and the highest absorption of 75.82% were obtained in the BaM x = 0.6 phase over the frequency range 9.66-10.93 GHz.

References

A. Doyan, Ilham H., Susilawati S. 2015. Pengaruh Variasi Temperatur Kalsinasi Terhadap Barium M-heksaferit Didoping Zn Menggunakan Fourier Transform Infra Red. Jurnal Pengkajian Ilmu dan Pengajaran Matematika dan Ilmu Pengetahuan Alam. DOI: 10.29303/jpm.v10i1.9, 10(1), pp. 7-13.

A, M. Cholifah. 2018. Master Thesis, Departement of Material Physics, Faculty of Natural Sciences, Sepuluh Nopember Institute of Technology, Indonesia.

Ataie and S. Zojaji. 2007. Synthesis of barium hexaferrite nanoparticles via mechano-combustion route“, Journal of Alloys and Compounds, vol. 431, no. 1-2, p. 331–336.

Awalin, N. 2017. Studi Penyerapan Gelombang Elektromagnetik Rentang X-Band Dengan Menggunakan Penyerap PANi Konduktif dan Barium M-HeksaFerrit Terdoping Ion Zn (0,3 ≤ X ≤ 0,9). Institut Teknologi Sepuluh November, Surabaya, Indonesia.

Bahtiar, Syamsul. 2010. *Pengaruh Doping Zn Terhadap Resistivitas Senyawa Spintronik ZnXFe2-xO3 Dengan Metode Coprecipitation*. Universitas Negeri Malang : Malang.

H. Li, L. Zheng, D. Deng et al. 2021. Multiple Natural Resonances Broaden Microwave Absorption Bandwidth of Substituted M-type Hexaferrites. Journal of Alloys and Compounds. https://doi.org/10.1016/j.jallcom.2021.158638.

H. Syahrul, Ratna A. S., Tua Raja S., S. Dermayu, & Perdamean S. 2015. Magnetic Properties of Cu^{2+} Substituted $BaFe_{12-x}Cu_xO_{19}$ (x= 0.1,0.2,0.3,...,4). Indonesian Journal of Applied Physics. ISSN:2089 – 0133, vol. 5, no. 1, pp. 71-78.

Joon, Y., Nishida K., Yamamoto T., Ueda S., Deguchi T., 2008. Charateritic Evaluation of Microwave Absorber Using Dielectric and Magnetic Composite Materials. *Journal of Ceramic Processing Research*. Vol. 9, No.4 pp 430-436.

K. Lee, J. C. Sur, I.-B. Shim, and C. S. Kim. 2009. The effect of manganese substituted M-type hexagonal Ba-ferrite", Journal of Magnetics, vol. 14, no 2, pp. 93-96.

K. S. Moghaddam and A. Ataie. 2006. Role of intermediate milling in the processing of nano-size particles of barium hexaferrite via co-precipitation method. Journal of Alloys and Compounds, vol. 426, no. 1-2, pp. 415-419.

Malhotra, S., M. Chitkara, & I.S. Sandhu. 2015. Microwave Absorption Study of Nano Synthesized Strontium Ferrite Particles in X Band. *International Journal of Signal Processing, Image Processing and Pattern Recognition*, 8 (10), pp.115-120.

Manawan, Maykel, A. Manaf, B. Soegijono, & A. Y. Hercuadi. 2014. Microstructures, Magnetic Properties and Microwave Absorption Characteristics of Ti^{2+} -Mn^{4+} Substituted Barium Hexaferrite. Jurnal Elektronika dan Telekomunikasi. Doi: 10.14203/jet.v14.15-19.

Ma'rifat, L.D. 2019. Undergraduate Thesis, Departement of Physics, Faculty of Natural Sciences, University of Halu Oleo, Indonesia.

M. Han, Y. Ou, W. Chen, and L. Deng. 2009. Magnetic properties of Ba-M-type hexagonal ferrites prepared by the sol–gel method with and without polyethylene glycol added", Journal of Alloys and Compounds, vol. 474, no. 1-2, p. 185–189.

Rafeekali, K., M. Maheen, & E.M. Mohammed. 2015. Influence of Rare Earth (Tb^{3+}) on Electrical and Magnetic Studies of Nickel ferrite Nanoparticles. *IOSR Journal of Applied Physics (IOSR-JAP).* ISSN: 2278-4861, 7(3), pp. 21-25.

Sahlam, A. Doyan, Susilawati. 2018. Sintesis Bahan M-Heksaferit Substitusi Logam Kobalt-Mangan dengan Metode Kopresipitasi. Jurnal IPA dan Pembelajaran IPA (JIPI). https://doi.org/10.24815/jipi.v2i2.12073, vol. 2, no. 2, pp. 64-68.

Sholihah, F.R., Zainuri, M. 2012. Pengaruh Holding Time Kalsinasi Terhadap Sifat Kemagnetan Barium M-Hexaferrite ($BaFe_{12-x}Zn_xO_{19}$) dengan Ion Doping Zn. *Jurnal Sains Dan Seni ITS*,) ISSN: 2301-928X, 1(1), pp. 25–29.

Priyono & W. G. Prasongko. 2013. Pembuatan Material Magnetik Komposit $BaFe_9Mn_{0,75}CO_{0,75}Ti_{1,5}O_{19}$ / Elastomer untuk Aplikasi Penyerap Gelombang Elektromagnetik. Jurnal Sains dan Matematika. 21(1), pp. 15-19.

Pullar, R.C., 2012. *Hexagonal ferrites: A review of the synthesis, properties and applications of hexaferrite ceramics.* Prog. Mater. Sci. 57. 1191–1334.

Ramadhan, M. I., Wahyu, W. & Sunardi, 2018. Pengaruh Temperatur *Sintering* Terhadap Struktur dan Sifat Magnetik Ni^{2+}-Barium Ferit Sebagai Penyerap Gelombang Mikro.*Jurnal Teras Fisika*.1.(1):26-27.

R. C. Pullar, "Hexagonal ferrites: A review of the synthesis, properties and applications of hexaferrite ceramics", Progress in Materials Science, vol. 57, p. 1191–1334, 2012.

S. Chaudhury, S. Rakshit, S. Parida, Z. Singh, K. S. Mudher, and V. Venugopal. 2008. Studies on structural and thermo-chemical behavior of $MFe_{12}O_{19}$(s) (M = Sr, Ba and Pb) prepared by citrate–nitrate gel combustion method", Journal of Alloys and Compounds, vol. 455, no. 1-2, pp. 25-30.

Seifert, J. Topfer, F. Langenhorst, J. M. LeBreton, H. Chiron, and L. Lechevallier. 2009. Synthesis and magnetic properties of Lasubstituted M-type Sr hexaferrites", Journal of Magnetism and Magnetic Materials, vol. 321, pp. 4045-4051.

Simbolon, Silviana, & Ahmad M. S. 2019. Sintesa dan Karakterisasi Material Komposit Berbasis BaO.6Fe2O3-C Sebagai Komponen Motor Listrik. Journal of Technical Engineering (PISTON), ISSN: 2541-3511, vol 3, no. 1, pp. 24-29.

Sulistyo, Indra M., & Priyono. 2012. Synthesis and Characterization of Magnetic Materials Barium Hexaferite Magnetic by Sol-Gel Theory as Microwave Absorption on X-band Frequency. Berkala Fisika. ISSN: 1410-9662, vol. 15, no. 2, pp. 63-68.

Suntoro, Achmad., R. N. Siregar, H. Nurcahyadi & L. Yuniarsari. 2021. A Study Operational Electromagnetic Compatibility (EMC) Testing Laboratory for Nuclear Equipment. PRIMA. Vol. 18, No. 2, pp. 8-17.

Tripathi, et al. 2015. Microwave Absorption Properties of Ni-Zn Ferrite Nano-Particle Based Nano Composite. *International Journal of Advanced Research in Science, Engineering and Technology*. 2 (2), pp. 463–468.

U. Topal, H. Ozkan, and L. Dorosinski. 2007. Finding optimal Fe/Ba ratio to obtain single phase $BaFe_{12}O_{19}$ prepared by ammonium nitrate melt technique, Journal of Alloys and Compounds, vol. 428, pp. 17-21.

Wirapraja, A. Y., & Ika P. W. 2018. The Effect of Charging Condition for Conducted Emission value of Information Technology Equipment. Widyariset, vol.4 (1). http://doi.org/10.14203/widyariset.4.1.2018.103-112.

Zebua, Y. B. 2018. Analysis of Crystal Structure and Magnetic Character Strontium Ferrite (SrFe12O19) Powder Made In Stoiciometry and Non-Stoiciometri Composition. Undergraduate Thesis, Departement of Physics, Faculty of Natural Sciences, University of Sumatra Utara, Indonesia.

Copyrights

Copyright for this article is retained by the author(s), with first publication rights granted to the journal.

This is an open-access article distributed under the terms and conditions of the Creative Commons Attribution license (http://creativecommons.org/licenses/by/4.0/).